Available online at www.sciencedirect.com
SCIENCE DIRECT®
ELSEVIER
International Journal of Thermal Sciences 42 (2003) 647–655
International Journal of Thermal Sciences
www.elsevier.com/locate/ijts

Bubble tracking in image sequences

Da-Chuan Cheng *, Hans Burkhardt

Institute of Pattern Recognition and Image Processing, Department of Computer Science, University of Freiburg, 79110 Freiburg, Germany

Received 7 May 2002; accepted 26 July 2002

Abstract

In this paper, we develop a system which can track bubbles in image sequences based on a manually selected initial contour of a bubble. The contours of bubbles are assumed to have circular shapes. Radial scans are used to characterize the position of each bubble. Based on specially selected features, contours of bubbles in subsequent images can be automatically tracked. This novel method reveals to be rather robust and produces good results also under difficult illumination conditions or with reflections on the surface of bubbles. Furthermore, based on a criterion which evaluates the situation of overlapped bubbles, the system can also deal with the overlapping problem and identify the bubbles correctly. After tracking, some parameters such as the bubble departure diameter, bubble flow speed, and bubble volume can be estimated which are important to investigate the heat transfer in a boiling system.

Keywords: Bubble tracking; Edge detection

1. Introduction

The aim of our cooperating research group [1,2] is to explore the heat transfer relationship between given liquids and heated tubes with different sizes, materials, and surface structures. The eventual goal is to discover the optimal heat transfer in order to save energy. For this purpose, many experiments are made and the processes are recorded with a high-speed digital video camera. The images are saved digitally with a resolution of 512 by 512 pixels. The sampling rate is 1000 frames per second. These experiments are made under different testing conditions such as liquid categories, tube materials, surface structures, pressures and heat fluxes, and temperatures. These factors have an influence on the quality of the recorded images. See Fig. 1. Fig. 1(a) is a middle-bottom view of a heated tube, the parameters of this experiment are: tube diameter 8 mm, $p_s = 4.24$ bar, $q = 1500$ W·cm^{-2}, emery ground surface type, propane. Fig. 1(b) is a bottom view of another tube, their parameters are: tube diameter 25 mm, $p_s = 4.74$ bar, $q = 3000$ W·cm^{-2}, sandblasted surface type, 2-propanal. There were two to three lamps for the illumination, the distance between the tube and the lamps is about 20 cm.

* Corresponding author.
E-mail address: cheng@informatik.uni-freiburg.de (D.-C. Cheng).

There are basically two major problems in the bubble identification [3,4]: the geometric problem and the optical problem. In the geometric problem, there are three sub-problems:

(1) The shape of the bubbles is dependent of the amount of the pressure and the heat flux.
(2) Two or more bubbles can merge together to form a larger one. During the merging process, the shape of the bubbles varies and is unpredictable.
(3) The bubble attached to the tube surface can be covered by another one which is flowing upwards.

In the optical area, there are four sub-problems:

(1) The reflections on the surface of the bubbles show large variations in different image sequences. They even vary in different positions within the same image sequence.
(2) The reflection can happen not only on the bubbles, but also on the background, i.e., the tube. This phenomenon gives rise to noise. See Fig. 1(a).
(3) There are some shadows accompanied the larger bubbles or the flowing smaller ones. The shadows are sometimes similar to bubbles in both gray value and texture. This makes the identification very difficult.

1290-0729/03/$ – see front matter
doi:10.1016/S1290-0729(03)00030-9

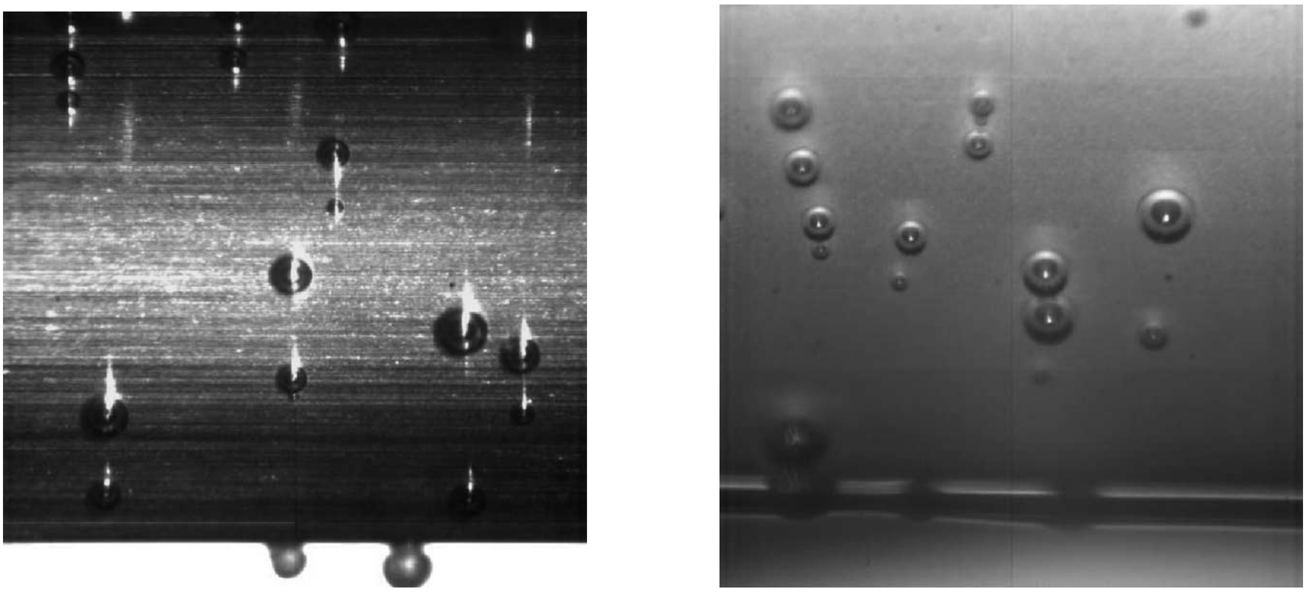

(a) (b)

Fig. 1. Two kinds of image sequence: (a) there are some strong reflections on the bubbles and on the tube. The upper and lower part of the image are in a lower contrast; (b) the reflections are principal on bubble surfaces, however, there are strong shadows under the bubbles since the light source is from the upper position. The experimental conditions of these two image sequences are described in Section 1.

(4) Some bubbles are in a low-contrast area. This phenomenon happens on the top or the bottom of the tube because of less illumination due to the curvature of the tube.

All of the above possibilities make bubbles quite different in geometry and in appearance and difficult to be identified. Noticeably, bubbles are inhomogeneous in gray values. Therefore, segmentation methods based on the histogram are not suitable in this application.

In this study, we treat experiments which are made under an intermediate pressure and at low heat flux. Under this condition, bubbles are mostly circular especially the smaller ones. Consequently, the circular model can be applied to estimate the shape of the bubbles. The advantages of using a circular model are: (1) Since there are some unpredictable reflections on the surface of bubbles and on the tube, some boundary information are lost. See Fig. 1(a). Moreover, the reflection might move while the bubble is moving upwards. This means that boundary surrounding information might be changed or lost in different time instances. Therefore, the tolerance of error becomes important in tracking bubbles. The circular model provides us the ability to tolerate such unavoidable errors. (2) Another error appears when the bubble to be tracked is covered by another flowing bubble. In this situation, part or even the whole bubble information is lost. With the help of a circular model, the boundary can be reconstructed based on the proposed method and a circular model. In this paper, we propose a method that can deal with the optical problems under the prerequisite of a circular model. The details of the system are described in Section 2.

2. System architecture

For the intention to deal with all the optic problems, some prior knowledge is apparently necessary. Since our goal is to identify the bubble contour accurately, the surrounding boundary information is very important. The system needs a manually selected contour as initialisation. A bubble at a nucleation site is selected via a GUI (graphic user interface) [5] by giving at least 3 points on the bubble contour. A least square error minimization process is used to get the optimal circular shape [6]. Since the intensities around the bubble contour are changing in different images, the initial contour is used only once in detecting the bubble in the next image. In detecting bubbles in subsequent images, their previous results are applied.

Once the system obtains the primitive contour, it assumes that the bubble is growing. The volume of the bubble should not decrease. The local information surrounding the contour is the only information that the system has. It is notable that the single gradient information is not suitable for this application. This is due to several reasons:

(1) there are many strong reflections near the inner or outer contour of the bubble in some image sequences;
(2) the bubble might have no reflection in the beginning, after some formation, the reflection appears;
(3) there are sometimes strong shadows accompanying the bubble.

All of these possibilities influence the use of gradient values and cause ambiguities in identifying the contour. To maintain the local information around the contour is

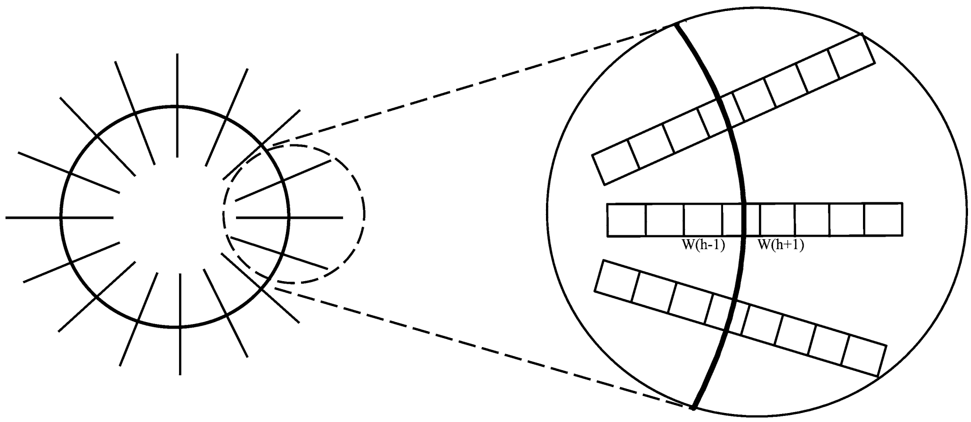

Fig. 2. An example of the 16 radial lines on the contour and their corresponding component arrays. The left circle is a bubble boundary. The right circle is a part from the bubble boundary. The radial scans are composed by the component arrays which contain the local boundary information.

nontrivial. Our solution is using a cost function which is a combination of the gradient direction, a comparison between two vectors, and some weighting factors to determine the optimal position where the contour is.

For a bubble $\boldsymbol{B}$, let (x_m, y_m) denote the geometric middle point of the primitive contour $K_P = \{(x_k, y_k) \mid k = 1, 2, \ldots, n\}$ in image I_{i-1}. 16 or 32 points from K_P are selected which should be equally distributed on the contour. The reduction is a sampling on the contour in order to reduce the computation time. The selected number of points depends on the contour length. If the length is larger, 32 points are applied. These points will replace the whole contour points to represent a bubble. Gray level pixels under a radial line which crosses a selected point compose a 1D array, which we name component array. See Fig. 2.

The tracking process is divided into two steps: the determination of bubble movement and the contour identification. The reasons for determining bubble motions are:

(1) If there are some turbulences resulting from other flowing bubbles, the growing bubble will vibrate.
(2) Some bubbles reveal a helix type movement.

Via this process, the system can detect the position of the bubble roughly. Afterwards, the contour identification follows.

2.1. Determination of bubble motion

In order to determine the motion of a bubble, a comparison between the identified bubble in the previous image I_{i-1} and a searching region in the current image I_i is applied. We implement it by calculating the gray level difference. Since part of the bubble changes in gray level during the bubble formation, it is intuitive to give an error tolerance to deal with this situation. A function is defined, i.e.,

$$F(\Delta x, \Delta y) = \sum_{\forall (x_c, y_c) \in \Omega_{i-1}} f_{x_c, y_c}(\Delta x, \Delta y) \qquad (\Delta x, \Delta y) \in S \tag{1}$$

where

$$f_{x_c, y_c}(\Delta x, \Delta y) = \begin{cases} 1 & \text{if } \left| g_i(x_c + \Delta x, y_c + \Delta y) \right. \\ & \quad \left. - g_{i-1}(x_c, y_c) \right| \leqslant T \\ 0 & \text{otherwise.} \end{cases}$$

Δx and Δy are translations in x and y direction, respectively. S denotes the searching region on image I_i. $g_i(x, y)$ is the gray level at position (x, y) on image I_i. $(x_c, y_c) \in \Omega_{i-1}$ represent the coordinates of all points in the bubble in image I_{i-1}. $T = 4$ is a threshold. The translations search the possible region where the bubble might be. One value, $F(\Delta x, \Delta y)$, is obtained for each translation $(\Delta x, \Delta y)$. The bubble middle point (x'_m, y'_m) in image I_i can be determined when F reaches its maximum. In this study, the searching region is limited to a few pixels, i.e., $-6 \leqslant \Delta x \leqslant 6$ and $-2 \leqslant \Delta y \leqslant 6$. The lower bound for Δy is less since the bubble do not move downwards except the helix type motion. After the motion determination, the previous bubble is placed on current image I_i with the new middle point.

2.2. Contour identification

Let the component arrays denote as $\{\boldsymbol{w}_j \mid j = 1, 2, \ldots, n\}$, where n is the number of radial lines which is either 16 or 32. They contain the local information around the bubble contour. Due to the fact that there are possible gradient changes on the contour, a feature which represents the gradient information is defined:

$$e_j = \sum_{k=h-1}^{h} w_j(k) - \sum_{k=h+1}^{h+2} w_j(k) \tag{2}$$

where $w_j(h)$ is the corresponding contour point in the component array $\boldsymbol{w}_j$. Here we consider the gradient change only along the direction of the radial line. Therefore, a cost function can be defined:

$$C_{j,i} = \frac{1}{N} |w_{j,i-1} - w_{j,i}|^2 - e_{j,i} e_{j,i-1} W_g \tag{3}$$

where W_g is a scalar that can be chosen by the user acting as a weighting factor. A translation on each radial line is applied:

$$C_{k,j,i} = \frac{1}{N}|w_{j,i-1} - w_{k,j,i}|^2 - e_{j,i-1}e_{k,j,i}W_g \tag{4}$$

where $-1 \leqslant k \leqslant R$ is an index of translation along radial line j. $k = 0$ indicates the corresponding contour position on image I_{i-1}. R is either 3 or 6 pixels that can be chosen by the user. If there are more heat flux or less pressure, the bubble grows quicker and the larger search region is applied. An optimal solution is found if, $C_{h,j,i} = \min(C_{k,j,i})$ for $-1 \leqslant k \leqslant R$.

The corresponding position h is a candidate on the radial line j. The whole candidates of the radial lines are used to form a bubble contour based on the circular model. The first item on the right-hand side of Eq. (4) plays a role as a comparison of two component arrays, which should reveal the movement of the boundary point and identifies the new contour position. However, according to our experiences, this is not enough since the gray level around the contour might be changed. To commute the insufficiency, feature e is added. This feature captures the gradient if any. If there is a large gradient on the boundary, feature e dominates the cost value. On the contrary, it reduces its effect or even vanishes and lets the other feature be dominant. Moreover, if the gradient directions are different between $e_{j,i-1}$ and $e_{j,i}$, the cost value is increased and the possibility to be a candidate is decreased. The advantage of this method is that it uses an adaptive comparison method instead of the traditional correlation.

2.3. Overlap detection

The overlap or occlusion of bubbles causes problems in motion determination and contour identification. Specifically, it is difficult to track the bubble if it is overlapped or covered by the other flowing bubble and meanwhile it is growing. This situation happens often if there is much heat flux from the tube. Therefore, it is necessary to detect whether there is such a situation. Fig. 3 are sub-images from original images. From (a) to (d) are sequential images which demonstrate that the bubble to be tracked (in the middle) is overlapped by another large flowing bubble (on the right-hand side). Firstly, the image where the bubble appears again should be determined, then, the estimations of bubble contours during the occlusions can be interpolated.

Regarding the detection whether there is overlap or total occlusion, an intuitive method is comparison. If a bubble is overlapped by another one, the gray values in the overlapped part are changed. The gray level change larger than ± 4 is accumulated and its number is denoted as N_c. It is assumed to be overlapped if the ratio $N_c/N \leqslant 0.4$, where N is the total pixel number of the bubble. Once the system detects the overlap, it cannot use processes in Sections 2.1 and 2.2. Instead, a scheme is proposed to recognize the image where the bubble appears again. Intuitively, the comparison between the known bubble and the tested image can be applied. Unfortunately, the bubble might grow while it is overlapped. Therefore, the method in Section 2.1 can not be applied. Our strategy is to compare the bubbles not in the spatial domain but in the frequency domain. Fig. 4(a) illustrates two signals with different sampling rates, i.e.,

$$y_i = \sin\left(2\pi f_1 \frac{t}{T_i}\right) + \cos\left(2\pi f_2 \frac{t}{T_i}\right) \quad \text{for } i = 1, 2 \tag{5}$$

where $f_1 = 5$, $f_2 = 3$, $T_1 = 100$, and $T_2 = 125$. The signal with a larger sampling rate simulates the growth of a bubble. Fig. 4(b) are the DFT (Discrete Fourier Transforms) of the corresponding signals. Notably, the frequency response is symmetric at $f = 50$ for y_1 and at $f = 63$ for y_2 in Fig. 4(b). The amplitudes at $f = 3$, $f = 5$ of y_1 indicate the frequencies of the signal. Since signals are same in frequency, there are also amplitudes at $f = 3$ and $f = 5$ of y_2. If we compare these two signals in the frequency domain by each element, there is nearly no difference. Fig. 4(c) illustrates the difference of two signals of length 100. This example demonstrates how we compare two bubbles in two images if the bubble grows. In addition, the brightness of the bubble might change if the bubble moves. In such a situation, the difference appears only at $f = 0$ in the frequency domain indicating the shift of the signal on y-axis in the spatial domain. Fig. 5 illustrates this occasion. In summary, the cost function we used is:

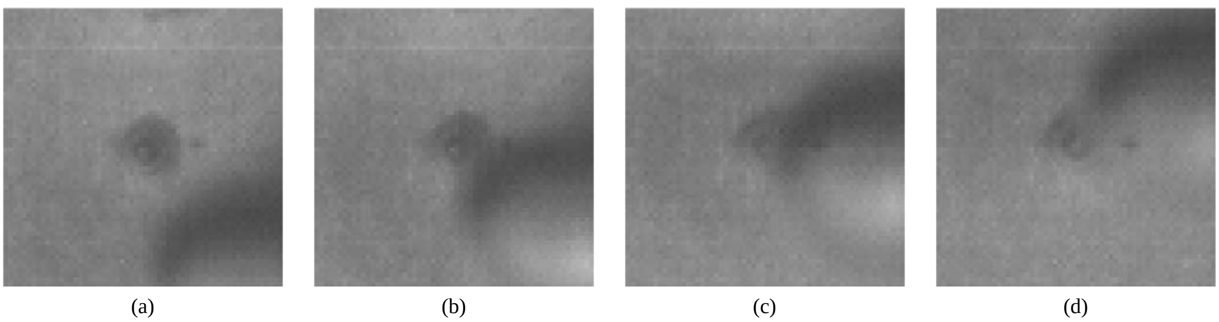

Fig. 3. A larger bubble (right) flows over the bubble to be tracked (in the middle). These images are sub-images from the image sequence shown in Fig. 1(b).

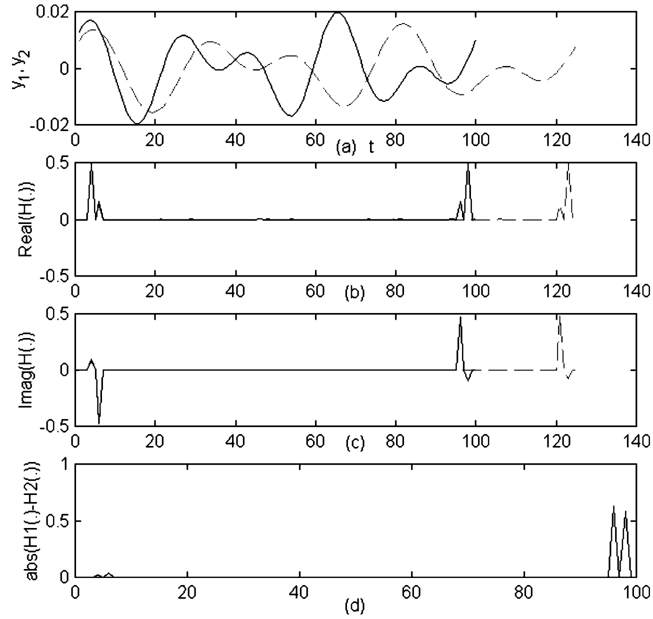

Fig. 4. (a) Two synthetic signals with the same frequency but different sampling rate. (See Eq. (5).) These two signals simulate the different length of the profile extracted from the bubbles of different radii. y_1 is denoted by the solid line; and y_2 by the dashed line. (b) The real part of the DFT of the signals y_1 and y_2, they are superimposed. (c) The imaginary part of the DFT of these two signals, they are superimposed. (d) The difference of their frequency responses. There is no difference between index 0 and 50.

$$S(i+\Delta i) = \min_{\substack{\Delta x,\Delta y\in\Omega\\ 0\leqslant\Delta r\leqslant 4}} \sum_{h=1}^{2}\Big[\Big(\mathrm{Re}\,al\big(\boldsymbol{H}\big(\boldsymbol{g}_h(x+\Delta x, y+\Delta y, r+\Delta r, i+\Delta i)\big)\big) - \mathrm{Re}\,al\big(\boldsymbol{H}\big(\boldsymbol{g}_h(x,y,r,i)\big)\big)\Big)^2 + \Big(\mathrm{Im}\,ag\big(\boldsymbol{H}\big(\boldsymbol{g}_h(x+\Delta x, y+\Delta y, r+\Delta r, i+\Delta i)\big)\big) - \mathrm{Im}\,ag\big(\boldsymbol{H}\big(\boldsymbol{g}_h(x,y,r,i)\big)\big)\Big)^2\Big] \quad (6)$$

where $\boldsymbol{g}_h$ is the feature vector extracted from the bubble defined below. $\mathrm{Re}\,al(\boldsymbol{H}(\boldsymbol{g}_h))$ and $\mathrm{Im}\,ag(\boldsymbol{H}(\boldsymbol{g}_h))$ are the real and imaginary part of the DFT of $\boldsymbol{g}_h$, respectively. x, y are indices of the x and y-coordinate; r is the radius of the bubble. i is the image index indicating the image number without overlap. $i+\Delta i \in N$ indicate image numbers with occlusion. The system searches the bubble in a local region defined by the translations Δx, Δy with different radii $r+\Delta r$. It compares feature vectors in the local region of the test image $i+\Delta i$ with the known feature vector $\boldsymbol{H}(\boldsymbol{g}_h(x,y,r,i))$. The length of the feature vector $\boldsymbol{H}(\boldsymbol{g}_h(\bullet))$ depends on the radius, $r+\Delta r$, of the bubble. Here we define the feature vector:

$$\boldsymbol{g}_1(x,y,r+\Delta r) = \frac{1}{2(r+\Delta r+\eta)+1}\big\{f(x+k,y)-f(x+k-1,y) \mid -r-\Delta r-\eta \leqslant k \leqslant r+\Delta r+\eta,\ k\in Z\big\}$$

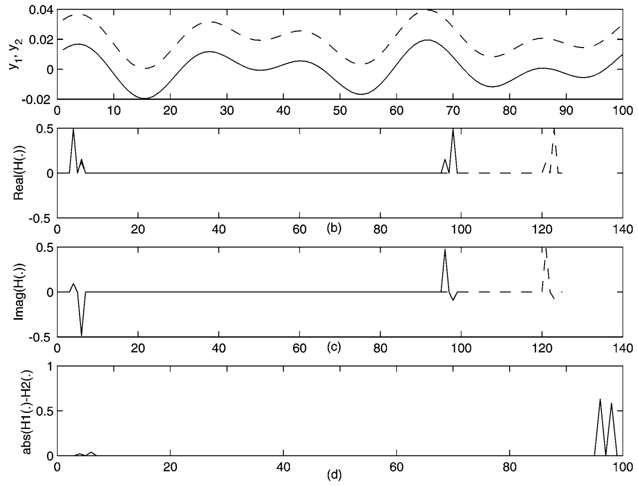

Fig. 5. (a) Two synthetic signals are same in frequency but different in amplitude. These signals simulate the profiles extracted from two different bubbles with different intensities. (b) The real part of the DFT of these two signals. They are plotted superimposed. (c) The imaginary part of the DFT of these two signals, plotted superimposed. (d) The difference between the two signal in frequency domain.

$$\boldsymbol{g}_2(x,y,r+\Delta r) = \frac{1}{2(r+\Delta r+\eta)+1}\big\{f(x,y+k)-f(x,y+k-1) \mid -r-\Delta r-\eta \leqslant k \leqslant r+\Delta r+\eta,\ k\in Z\big\}$$

where $\Delta r \geqslant 0$ is the prediction of growth of the bubble $\eta = \frac{r}{3}$. $f(x,y)$ is the gray level at coordinate (x,y). (x,y) is the middle point of the bubble. $\boldsymbol{g}_1$ and $\boldsymbol{g}_2$ are actually the gradient of the 1D sampled profile on the bubble. The reason that we use the gradient of the profile instead of the profile as a feature because it can better characterize the bubble information. We take only two samples of two different directions because of the reduction of computation time. Based on some experiments, we found they are sufficient to represent the whole bubble.

The subtraction in Eq. (6) is carried out by the elemental subtraction of the two vectors, $\boldsymbol{H}(\boldsymbol{g}_h(\bullet))$. Since the length of the feature vectors $\boldsymbol{g}_h$ might also be different, the length of $\boldsymbol{H}(\boldsymbol{g}_h(\bullet))$ might be different. We choose elements in a certain range. For instance, if the length of the known feature vector $\boldsymbol{g}_h$ is 100, then the length of $\boldsymbol{H}_{\text{known}}(\boldsymbol{g}_h)$ is also 100. We choose the elements between index 1 and 50 from $\boldsymbol{H}_{\text{known}}(\boldsymbol{g}_h)$ and compare it to the test vector $\boldsymbol{H}_{\text{test}}(\boldsymbol{g}_h)$ with the same element range. Noticeably, the length of $\boldsymbol{H}_{\text{test}}(\boldsymbol{g}_h)$ is equal to or larger than that of $\boldsymbol{H}_{\text{known}}(\boldsymbol{g}_h)$. The difference of the two vectors are calculated, for every translation and different radius. One minimum cost value will be obtained for each image. The cost values are very high in the overlapping area and very low if the bubble appears again. Via this scheme, we can detect the position and the radius of the bubble which appears again after overlap or occlusion by choosing the image which has the minimum cost value defined in Eq. (6). The estimation of radius is:

$$r' = (r + \Delta r + \eta)\frac{r}{r + \eta} \tag{7}$$

where Δr is determined by choosing the minimum S value.

3. Results

Fig. 6 illustrates an example of an overlap. The bubble to be tracked is in the middle of the sub-images which is still and attached on the wall of the heated tube. A flowing bubble overlaps this bubble partially while it is passing through.

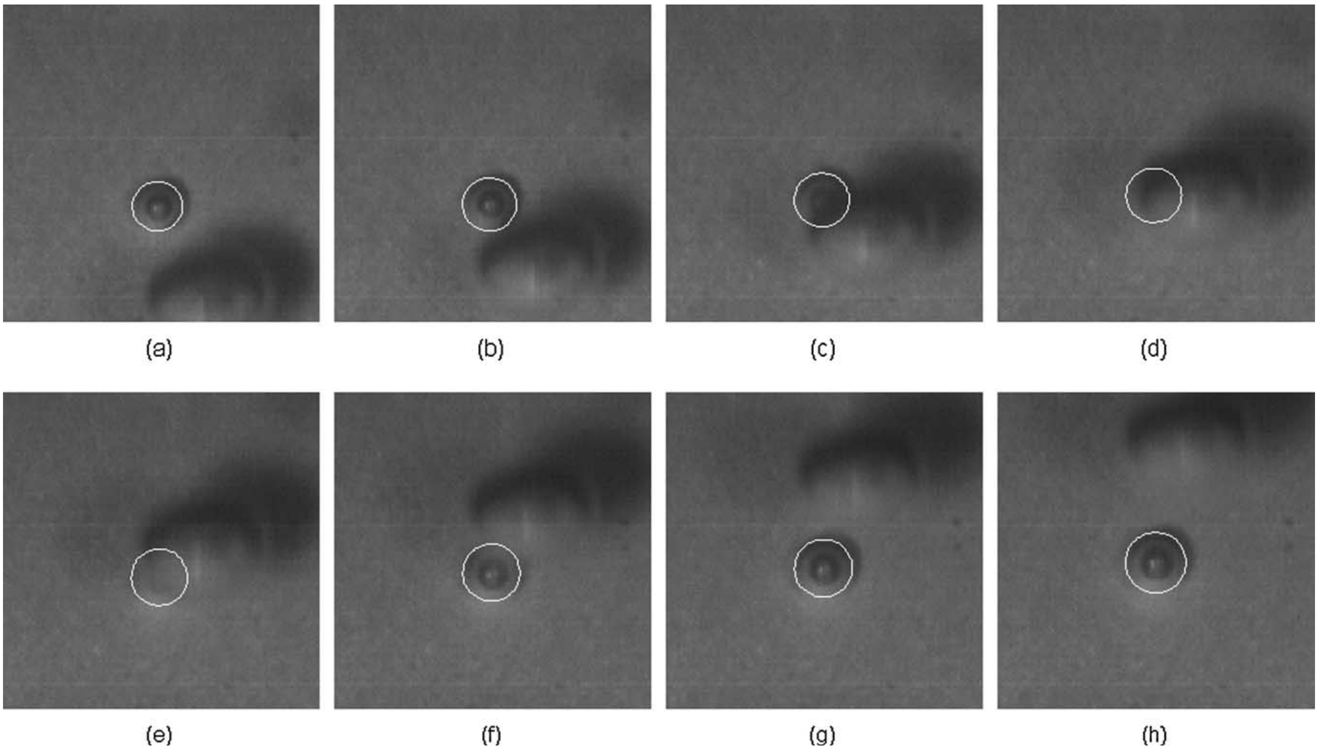

Fig. 6. An overlap example. From (a) to (h) are sub-images of a sequential image sequence shown in Fig. 1(b).

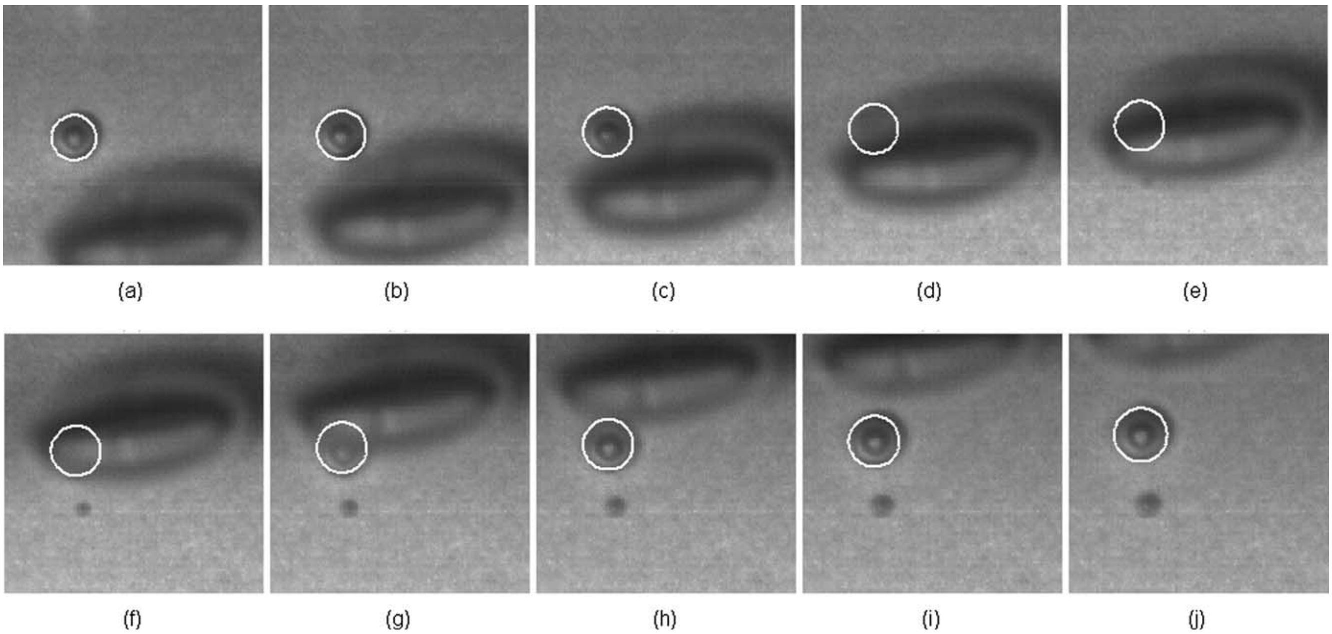

Fig. 7. An example of occlusion. From (c) to (h) are the linear interpolations between (a) and (i). They are sub-images from an image sequence which is a middle view on the same tube and with the same conditions to Fig. 1(b).

If there is no overlap, the radial scans are used to identify the boundary of the bubble. In this illustration, it is (a) to (b). The candidates of each radial scan are used to form a circle. The circles are the boundaries of the bubbles denoted as light lines which are superimposed on the sub-images. In Fig. 6(c), the system detects the overlap. The scheme in Section 2.3 is applied and Fig. 6(g) is determined where the bubble appears again. The boundaries of (c) and (f) are linear interpolations of (b) and (g).

Fig. 7 demonstrates an example of occlusion. In this illustration, the overlaps happen from (c) to (h). The system detects the overlap in (c) and uses (a) as the known information. We use (a) as a prior knowledge instead of (b) due to the consideration of robustness. This is because sometimes the bubble may have different illumination before it is covered. Via the proposed scheme, it detects (i) in which the bubble appears again. The contours from (c) and (h) are linear interpolations of the contours (b) and (i). Noticeably, the bubble to be tracked grows meanwhile when it is covered. Fig. 8 is a cost value plot. The abscissa indicates the images index and the ordinate is the minimum value calculated by Eq. (6) of each image. The values in Fig. 8 are the corresponding result in Fig. 7. The first value indicates image Fig. 7(c) and the seventh value indicates Fig. 7(i) where a global minimum is found.

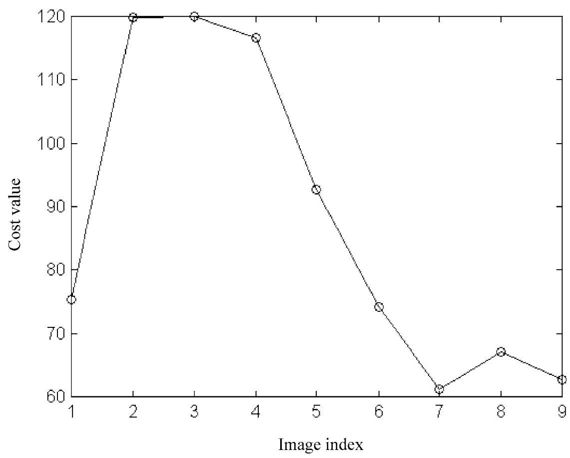

Fig. 8. A cost value plot of the searching process in the overlap detection in Section 2.3. The abscissa indicates the image index with respect to the images in Fig. 7, where index 1 indicates (c), index 2 indicates (d) and so on.

Fig. 9 is another example of occlusion. Two bubbles are flowing upwards and cover the bubble to be detected completely. This result illustrates that the system is able to detect the occlusion and to track bubbles fully automatically even if the bubbles are in a poor illuminated area. All of these illustrations demonstrate the ability of the proposed scheme in dealing with the overlapping/occlusion problem in tracking bubbles.

Some of our image sequences have strong reflections on bubble surfaces and on the tube. The tracking results regarding the image sequence from Fig. 1(a) are given in Fig. 10. There are strong reflections on the bubble surface and on the tube. Some boundary information is lost. The situation is even worse that the places of reflection are varied. Based on the help of a circular model, the system can tolerate some unavoidable errors and identify the correct boundary of the bubble and track bubbles automatically.

4. Discussion

The aim of this paper is to solve the optical problems mentioned in the introduction. These problems arise from

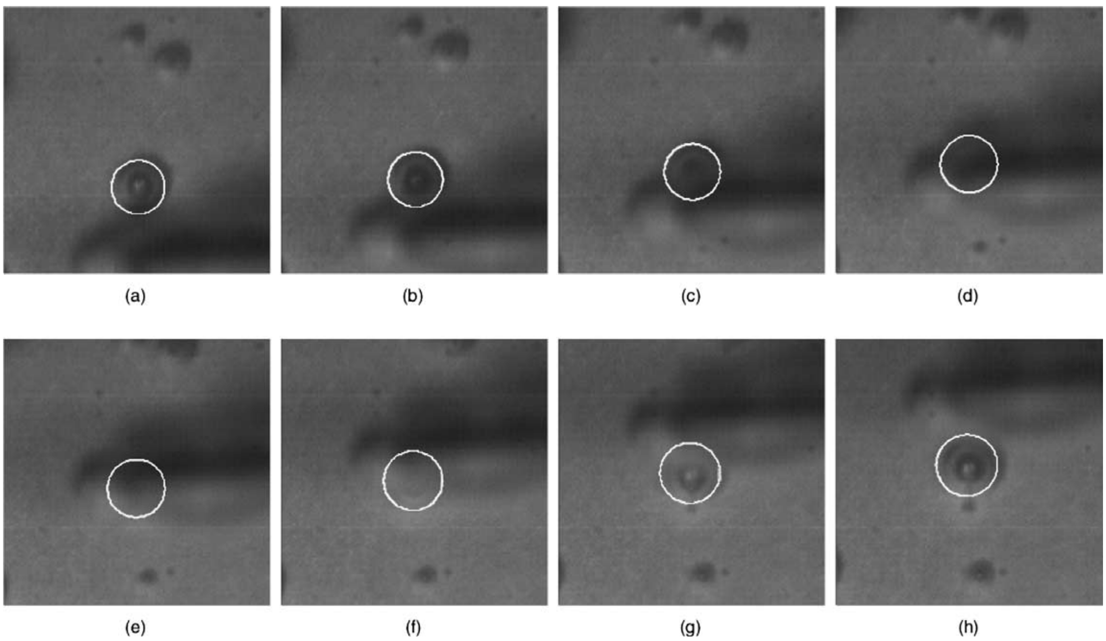

Fig. 9. Another example of occlusion. From (b) to (g) are the linear interpolations between (a) and (h). They are sub-images from the sequence shown Fig. 1(b).

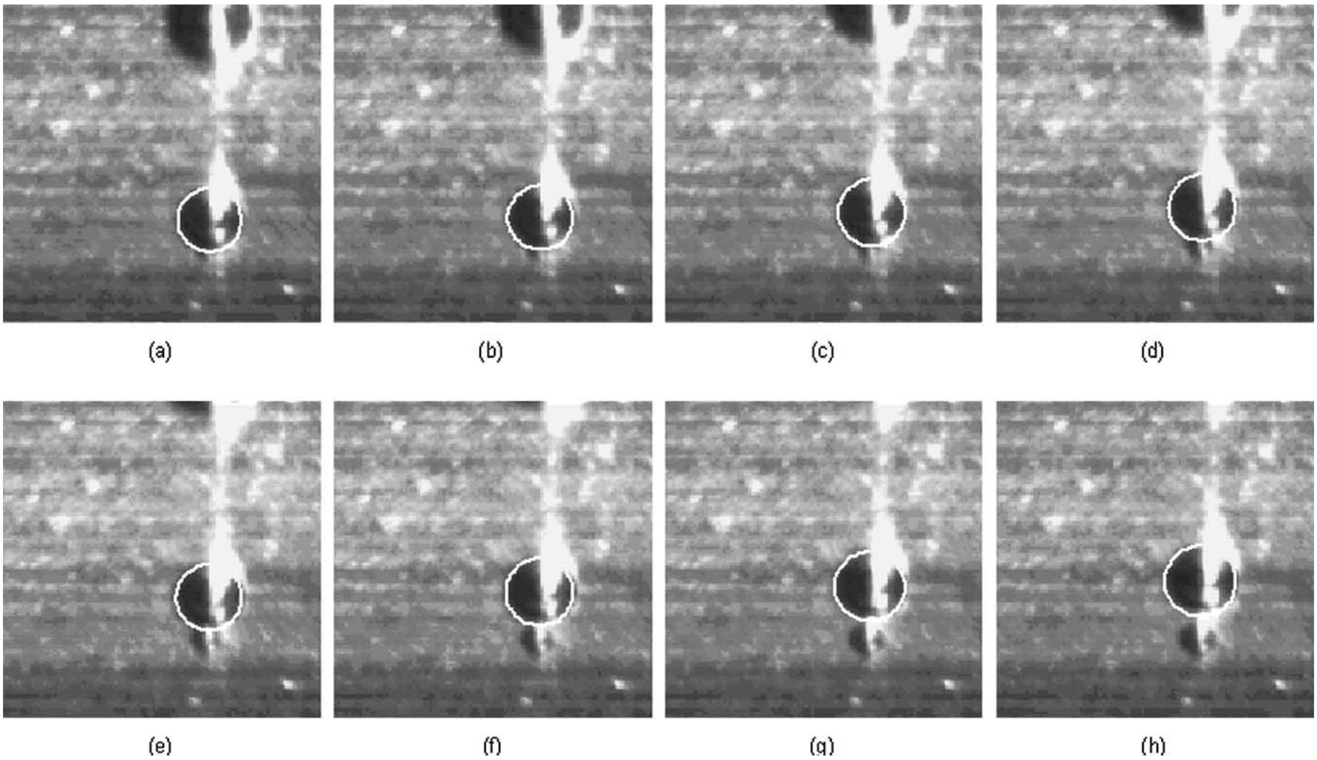

Fig. 10. The system tracks the bubbles in an image sequence illustrated in Fig. 1(a). There are strong reflections on the bubble surfaces and on the tube. The experimental conditions are the same to Fig. 1(a).

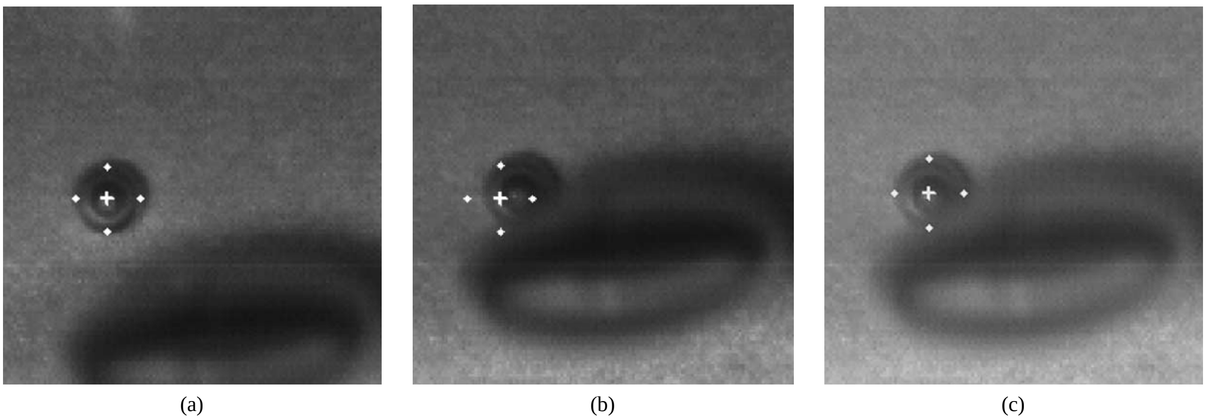

Fig. 11. (a) is the bubble before overlap and (b), (c) are bubbles in overlapping. The system uses the prior information of (a) and identifies the middle point and radius of the bubble in overlapping with different features (details in Section 4). The experimental conditions are the same to Fig. 1(b).

the reflections on the surfaces of bubbles and on the tubes. Moreover, since the illumination of the image is inhomogeneous, the gray level distribution on the bubble surfaces might change depending on their positions. Furthermore, the bubble might be in a poor-illuminated area resulting from the curvature of the heated tube. It is nontrivial to handle the bubble contour exactly. Specifically, the possibility of overlap or occlusion makes the tracking more difficult. The illustrated examples demonstrate the ability in recognizing overlapping situations and further in identifying the bubble contour even if the bubble grows during the overlaps.

The reasons that we use the gradient of profiles instead of profiles as features are:

(1) the frequency analysis using the DFT loses the spatial information. Using the gradient can compensate some loss of spatial information;
(2) the problem caused by the brightness shifts can be easily avoided.

According to our experiences, if the profiles are applied, some false identifications might happen. Fig. 11(a) is a bubble before the occlusion and is used as prior information as illustrated in Fig. 7(a). Fig. 11(b) and (c) are results of identifications by a gray level profile and gradient of the profile, respectively. The '+' denote the bubble middle points. The other four points surrounding the middle point represent the contour of the bubble. From the result, it is obvious that Fig. 11(c) is better than Fig. 11(b). There are still some other observations which reveal that the feature of the gradient of the gray level profile is better than the gray level profile but they are not shown here.

5. Conclusion

We propose a scheme to track bubbles in image sequences automatically, based on a manual selection as a primitive contour and under the assumption of a circular model. The system can track bubbles under difficult illumination conditions. Compared to our formal study [3], it has the ability to recognize the overlapping/occlusion situations and can identify bubbles when they reappear. During the overlap, the bubble might grow or move to another different illumination area. Based on the proposed scheme and a circular model, the bubble contour can be identified and reconstructed. Additional parameters after bubble tracking such as bubble diameter and bubble speed can be derived; they are especially important in exploring the heat transfer mechanism in a boiling system.

The future work is to explore how to identify the nucleation sites of vapor bubbles automatically. If the nucleation sites of an image sequence are known, they could offer the initial contours automatically which are given manually in this study.

Acknowledgements

The authors thank Prof. D. Gorenflo, University of Paderborn, for providing the bubble images. The first author thanks Dr. A. Luke and S. Rahmann for valuable discussions. This research is funded by grants of Deutsche Forschungsgemeinschaft (DFG).

References

[1] D. Gorenflo, W. Fust, A. Luke, E. Danger, U. Chandra, Pool boiling heat transfer from tubes with basic surface modifications for enhancement, in: E.W.P. Hahne, W. Heidemann, K. Spindler (Eds.), Proceedings of the 3rd European Thermal Sciences Conference, Edizioni ETS, Heidelberg, Germany, September, 2000, pp. 743–748.

[2] A. Luke, New methods of characterization for the microstructure of heated surfaces in boiling, in: E.W.P. Hahne, W. Heidemann, K. Spindler (Eds.), Proceedings of the 3rd European Thermal Sciences Conference, Edizioni ETS, Heidelberg, Germany, September, 2000, pp. 737–742.

[3] D.-C. Cheng, H. Burkhardt, Tracking bubbles in high-speed image sequences, in: International Conference of Thermophysical Properties and Transfer Processes of New Refrigerants, B5.4, Paderborn, Germany, October 3–5, 2001.

[4] D.-C. Cheng, H. Burkhardt, Bubble recognition from image sequences, in: Inverse Problems and Experimental Design in Thermal and Mechanical Engineering, Eurotherm Seminar N° 68, Poitiers, France, 5–7 March, 2001.

[5] D.-C. Cheng, H. Burkhardt, Model-based evaluations from bubble image sequences, DFG Interim Report, SP-27, December, 2001.

[6] W.H. Press, S.A. Teukolsky, W.T. Vetterling, B.P. Flannery, Numerical Receipts in C, Cambridge University Press, Cambridge, 1988.